

# A Simple and Low-cost Synthesis Strategy of LiFePO<sub>4</sub> Nanoparticles as Cathode Materials for Lithium Ion Batteries

Huiting Zhu, Cui Miao, Ruitong Guo, Ying Liu and Xingyao Wang\*

Department of Chemistry, School of Sciences, Tianjin University, Tianjin, 300350, China

\*E-mail: [wxyghw@163.com](mailto:wxyghw@163.com)

Received: 4 December 2020 / Accepted: 6 January 2021 / Published: 31 January 2021

---

In this work, pure LiFePO<sub>4</sub> nanoparticles have been synthesized by a one-step facile hydrothermal stripping method. This particular method is environmentally friendly and cost-effective, allowing the recycling of solvents. The preparation procedure involves an aqueous solution and an organic phase. The organic phase is naphthenic acid loaded with ferrous ion. Since the extraction process can purify ferrous ions, inexpensive industrial-grade FeSO<sub>4</sub>·7H<sub>2</sub>O can be used as a raw material. The aqueous solution contains H<sub>3</sub>PO<sub>4</sub> and LiOH. Pure LiFePO<sub>4</sub> nanoparticles were synthesized by stripping ferrous ion from the organic phase and reacting precipitation in aqueous phase. The effect of various parameters, involving PH value, reactant concentration, amount of reducing agent, temperature and time on the properties of LiFePO<sub>4</sub> was examined. By comparing the electrochemical properties of samples with different morphologies and particle sizes as cathode materials for lithium-ion batteries, the optimum LiFePO<sub>4</sub> nanoparticles exhibited a high specific discharge capacity of 156.1 mAh g<sup>-1</sup> at 0.1 C after 40 cycles, revealing their adequate cycling performance.

---

**Keywords:** Lithium iron phosphate; Lithium-ion batteries; Cathode materials; A one-step method

## 1. INTRODUCTION

Lithium-ion batteries have many excellent characteristics, such as high energy density, long cycle life, high capacity and low self-discharge rate, having a pivotal role in energy storage devices [1]. Olivine-type LiFePO<sub>4</sub> (LFP) is regarded to be the most promising cathode material for lithium-ion batteries due to its high voltage platform of about 3.45 V [2], high theoretical capacity (~170 mAh g<sup>-1</sup>), excellent thermal and cycle stability, and low cost [3]. The inherent low electronic conductivity (10<sup>-8</sup> ~10<sup>-9</sup> S cm<sup>-1</sup>) and lithium ion diffusivity (1.8×10<sup>-14</sup> cm<sup>2</sup> s<sup>-1</sup>) of LiFePO<sub>4</sub> results in an inferior rate capability, thus limiting the implementation of LiFePO<sub>4</sub> in high-powered battery assemblies [4-6]. Research efforts have been focused on improving the electrochemical performance of LiFePO<sub>4</sub> materials

by employing different approaches, such as particle size reduction [7], conductive material coating [8,9], ion doping [10,11] and new synthesis methods.

LiFePO<sub>4</sub> has been synthesized using different techniques. Among these, solid-state reaction method is usually employed [12-14]. However, the long-term high temperature calcination and the presence of impurities in the final product, leads to high production costs and poor electrochemical performance. In contrast, the liquid phase method can generally produce high-purity and small-sized LiFePO<sub>4</sub> particles, which are able to reduce the diffusion path of lithium ions and accelerate the transmission rate of Li<sup>+</sup>, thereby improving the electrochemical performance. However, the reported liquid-phase methods, such as the microwave-hydrothermal synthesis [15], the co-precipitation preparation [16] and the spray pyrolysis technology [17] suffer from high preparation cost, environmental pollution hazards and difficult control of the reaction, rendering difficult large-scale industrialization. To solve the above problems, we have developed a simple and economical hydrothermal stripping route to produce pure LiFePO<sub>4</sub> nanoparticles.

In particular, in this work, pure LiFePO<sub>4</sub> nanoparticles were prepared by one-step hydrothermal stripping method. Inexpensive and easily available ferrous salt, LiOH, phosphoric acid and organic extractant were used as raw materials. The morphology and particle size of the products can be easily adjusted and controlled. Meanwhile, the effect of PH, reactant concentration, amount of reducing agent, temperature and time on the synthesized LiFePO<sub>4</sub> was investigated. Moreover, a reaction mechanism describing the synthesis procedure followed is proposed. The hydrothermal stripping method proposed overcomes various major issues existed in other methods, such as the difficult control of the reaction, the long preparation process, the high cost, the non-recycle organic phase and aqueous solution. More importantly, electrochemical performance analysis of the as-prepared LiFePO<sub>4</sub> material, revealed that the sample synthesized by this particular method has adequate cycling performance.

## 2. EXPERIMENTAL PROCEDURE

**Synthesis:** 20 ml naphthenic acid and 10 ml isoctyl alcohol were initially added in the beaker and saponified with ammonia water. Then FeSO<sub>4</sub>·7H<sub>2</sub>O solution was poured under stirring, followed by the separation of two phase solution to obtain the organic phase loaded with ferrous iron. The aqueous solution was prepared with LiOH, ascorbic acid and 3 mol L<sup>-1</sup> H<sub>3</sub>PO<sub>4</sub> (the molar proportion of the LiOH:H<sub>3</sub>PO<sub>4</sub> was 1.2:1) dissolved in deionized water. Ascorbic acid acted as a reducing agent to prevent the oxidation of Fe<sup>2+</sup>. Subsequently, the aqueous solution and the organic phase were transferred to a stainless steel autoclave, and heated to different temperatures (120, 130, 140, 160, 180, 200, 220, 250 °C) for different time (1, 3, 5 h) with vigorous stirring. The obtained precipitate washed with deionized water and absolute ethanol several times. The resulting product was dried in an oven at 60 °C for 12 h.

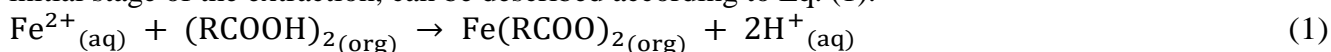
**Characterization:** The X-ray diffraction (XRD) of Cu-Kα radiation was used to identify the crystal of as-synthesized LiFePO<sub>4</sub> samples. Fourier transform infrared spectroscopy (FT-IR) (NEXUS 470 FT-IR spectrometer manufactured by Thermo) was used to gain insight into local structure. Rietveld refinement was used to analyze the lattice parameters and the average particle size of LiFePO<sub>4</sub>. Scanning

electron microscope (SEM, S-4800, made in Japan) was used to observe the morphology of LiFePO<sub>4</sub> samples.

Electrochemical measurements: CR2032 button half cells were manufactured in a glove box filled with argon. The 80 wt.% electrode material, 10 wt.% acetylene black and 10 wt.% polyvinylidene fluoride were uniformly dispersed in N-methyl-2-pyrrolidone (NMP). The formed slurry was coated on the Al foil and dried in oven at 80 °C to remove solvent NMP. The circular electrodes with a diameter of 14 mm were punched out from the foil and dried in a vacuum at 120 °C for 12 hours. Approximately 2 mg LiFePO<sub>4</sub> active material loaded on the foil. The separator used was polypropylene microporous membrane. The electrolyte was 1 M LiPF<sub>6</sub> dissolved in ethylene carbonate (EC)/diethyl carbonate (DEC)/ethyl methyl carbonate (EMC) (1:1:1 vol %). The galvanostatic charge/discharge test was performed with a multi-channel battery test system (LAND CT-2001A) at a voltage of 2.5 to 4.2 V. Cyclic voltammetry (CV) measurement were carried out from 2.5 to 4.2 V at a scanning rate of 0.1 mV s<sup>-1</sup> and electrochemical impedance spectroscopy (EIS) test at frequencies ranging from 0.01 Hz to 100 kHz were gathered in an electrochemical workstation (LK2010, LANLIKE).

### 3. RESULTS AND DISCUSSION

The process for synthesizing LiFePO<sub>4</sub> is schematically illustrated in Fig. 1. The reaction at the initial stage of the extraction, can be described according to Eq. (1).



Naphthenic acid with high thermal stability, low price, high extraction capacity and easy back extraction is selected as the organic extractant. In this process, the ferrous ions in solution were extracted into organic phase to form the organic phase loaded with ferrous iron.

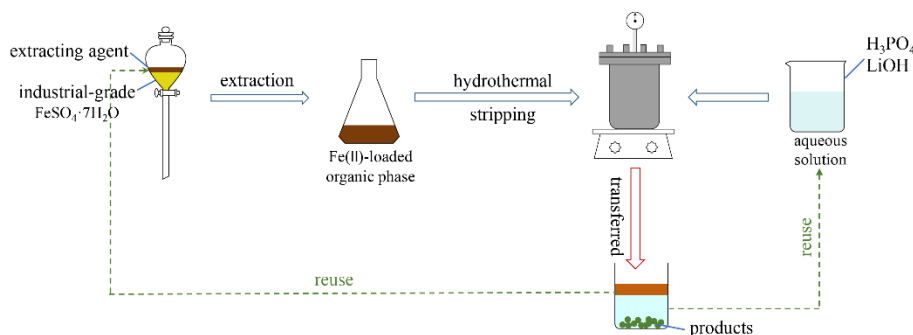
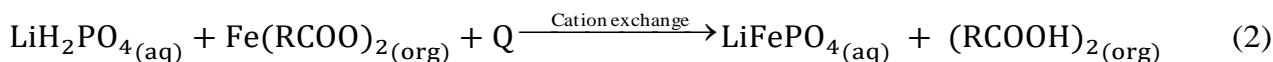


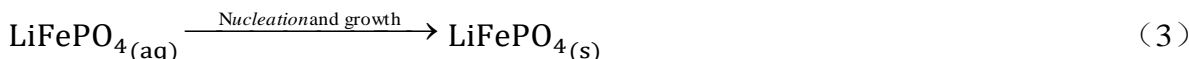
**Figure 1.** Hydrothermal stripping synthesis route.

Because the extraction process can purify ferrous ions, inexpensive industrial-grade FeSO<sub>4</sub>·7H<sub>2</sub>O can be used as a raw material. In the hydrothermal stripping stage, Fe<sup>2+</sup> was removed from the organic solution into the aqueous solution and reacted with Li<sup>+</sup> and PO<sub>4</sub><sup>3-</sup> to form LiFePO<sub>4</sub> precipitate.

Meanwhile, the naphthenic acid was released and can be reused. The mechanism of the hydrothermal stripping process can be described by Eq. (2).



Subsequently, the primary  $\text{LiFePO}_4$  crystals can nucleate and grow, according to Eq. (3).



After the reaction, the residual aqueous solution can return back to the stripping section.

Previous studies have found that different hydrothermal synthesis conditions, i.e. reactant's concentration, PH, amount of reducing agent, temperature and time can notably affect the formation and growth of  $\text{LiFePO}_4$  crystal [18]. In this regard, in the present work the effect of synthesis parameters on the properties of  $\text{LiFePO}_4$  particles synthesized by the hydrothermal stripping method, is thoroughly examined.

Fig. 2 shows the XRD patterns of  $\text{LiFePO}_4$  samples obtained with different  $\text{Li}^+/\text{PO}_4^{3-}$  molar ratios. The analysis confirmed that only when the molar ratio of  $\text{Li}^+/\text{PO}_4^{3-}$  was 1.2:1 (b), the pure and perfect crystal olivine  $\text{LiFePO}_4$  structure is obtained. Apparently, the choice of molar ratio has a great impact on the final product. When the ratio was low (a), structural defects in the crystal plane development can be obtained. When the ratio was high (c)-(e), impurity phases  $\text{Fe}_3(\text{PO}_4)_2(\text{OH})_2$ ,  $\text{Li}_3\text{Fe}_2(\text{PO}_4)_3$ ,  $\text{LiFe}(\text{PO}_4)(\text{OH})$ ,  $\text{Li}_3\text{PO}_4$  are observed. It can be concluded that  $\text{Li}^+/\text{PO}_4^{3-}$  ratio is one of the key factors for the synthesis of pure  $\text{LiFePO}_4$ . Moreover, a lower  $\text{Li}^+/\text{PO}_4^{3-}$  molar ratio was employed in the present work, as compared to the most hydrothermal synthesis methods which require a  $\text{Li}^+/\text{PO}_4^{3-}$  ratio of 3:1 [19], implying reduced lithium sources and in turn lower cost.

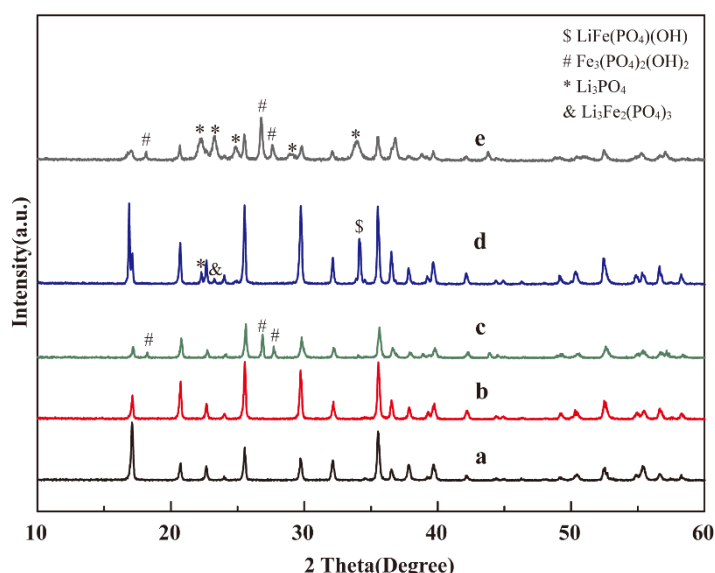


**Figure 2.** XRD of samples prepared with different  $\text{Li}^+/\text{PO}_4^{3-}$  molar ratio. (a) 1.1:1, (b) 1.2:1, (c) 1.3:1, (d) 2:1, (e) 3:1

Fig. 3 shows the XRD patterns of the synthesized samples at different PH values obtained by adjusting the amount of ammonia added. It can be clearly seen that samples (a)-(c) contain only a single phase  $\text{LiFePO}_4$  with an orthorhombic olivine structure (JCPDS no. 40-1499). This shows that pure

LiFePO<sub>4</sub> can be only obtained under acidic or neutral conditions. LiFePO<sub>4</sub> can't be obtained under basic conditions, since ferrous could be easily hydrolyzed to Fe(OH)<sub>2</sub> or Fe(OH)<sub>3</sub>, thus a mixture of Fe<sub>3</sub>O<sub>4</sub>, Fe<sub>2</sub>O<sub>3</sub> and lithium phosphate (Li<sub>3</sub>PO<sub>4</sub>) was obtained. These results were in line with the previous studies [20].

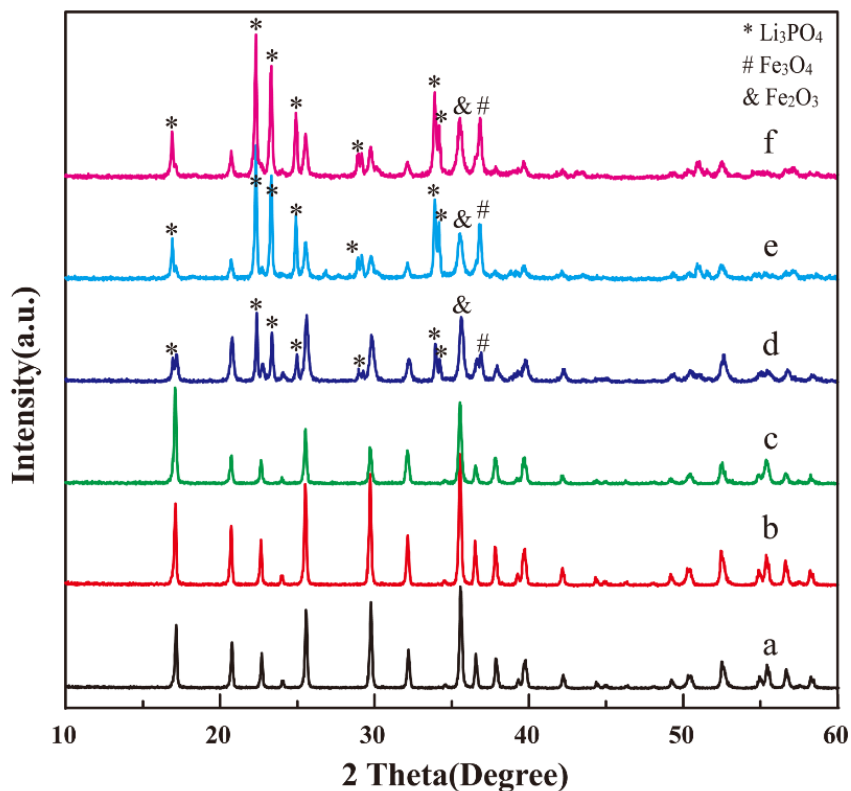


**Figure 3.** XRD of samples prepared under different pH values. (a) PH=5, (b) PH=6, (c) PH=7, (d)PH=8, (e) PH=9, (f) PH=10

Fig. 4 shows the XRD patterns of LiFePO<sub>4</sub> samples obtained with various amounts of reducing agent. In the synthesis process of sample (a), no reducing agent was added. The analysis showed that the product was Li<sub>3</sub>Fe<sub>2</sub>(PO<sub>4</sub>)<sub>3</sub>. It is obvious that Fe<sup>2+</sup> was oxidized to Fe<sup>3+</sup> during the reaction. The main characteristic diffraction peaks of the samples (b) and (c) are consistent with the LiFePO<sub>4</sub> phase, but there are some small diffraction peaks corresponding to LiFe(PO<sub>4</sub>)(OH). With the increase in the amount of reducing agent, the small impurity peaks in samples (d)-(g) disappeared, and the synthesized product was pure LiFePO<sub>4</sub> nanoparticles. This indicates that an appropriate amount of reducing agent is required in order to obtain pure phase LiFePO<sub>4</sub> sample [21-24].

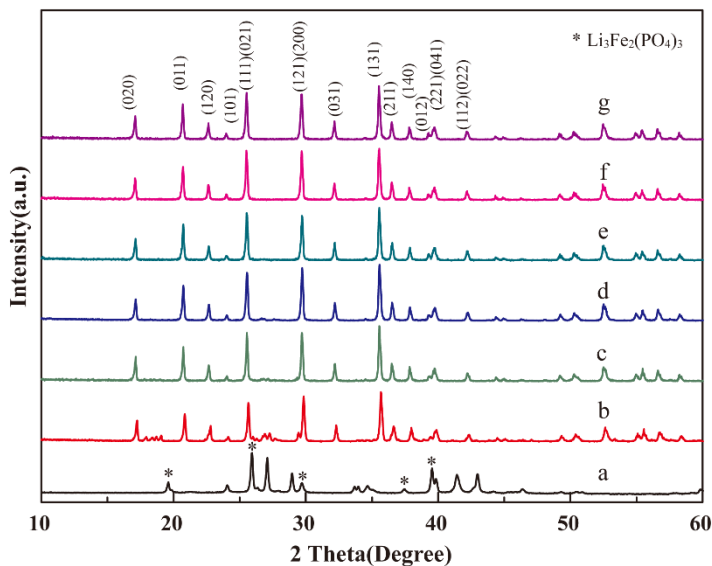


**Figure 4.** XRD of samples prepared with different reducing agent. (a) 0 %, (b) 1 %, (c) 2 %, (d) 3 %, (e) 4 %, (f) 5 %, (g) 15 %

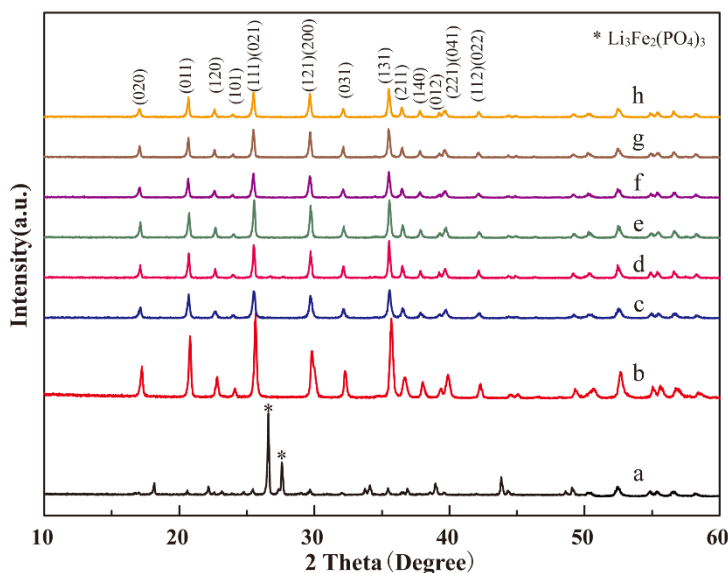


**Figure 5.** XRD of samples prepared under different reaction temperature. (a) 120 °C, (b) 130 °C, (c) 140 °C, (d) 160 °C, (e) 180 °C, (f) 200 °C, (g) 220 °C, (h) 250 °C

Fig. 5 shows the XRD patterns of  $\text{LiFePO}_4$  particles obtained at different temperatures. It can be observed that the two main diffraction peaks of the sample (a) prepared at 120 °C belong to  $\text{Li}_3\text{Fe}_2(\text{PO}_4)_3$ . As the reaction temperature increased to 130 °C, the characteristic peak of  $\text{LiFePO}_4$  appeared in sample (b). However, its main crystal plane development was quite different from the standard  $\text{LiFePO}_4$ , i.e. the (131) crystal plane diffraction peak dominates at the expense of (111) plane. When the temperature rose to 140 °C, the main crystal plane development of the sample (c) was consistent with the standard orthorhombic olivine structure of  $\text{LiFePO}_4$  pure phase (JCPDS no. 40-1499). This implies that the crystal

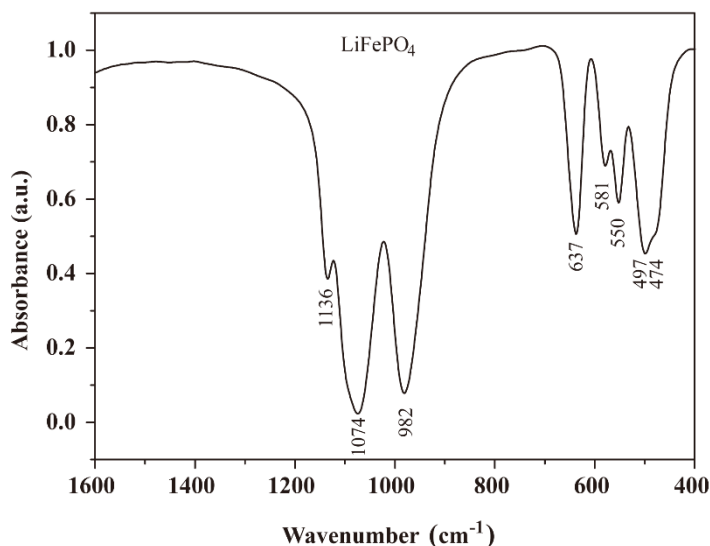
development is constantly improved during the heating process. When the reaction temperature reached 160 °C and above, the peak's intensity are progressively increased (samples d-h). This is due to the strong effect of temperature on formation of crystal nucleus and the consequent growth of crystals. High temperature can increase the vibration of atoms and the diffusion rate of crystal ions. Table 1 summarizes the unit cell parameters and average particle size calculated from the XRD results. It can be seen that the size of the synthesized nanoparticles initially increases gradually with the increase of temperature. When the temperature reaches 220 °C the growth is basically stops, followed by a decrease after reaching 250 °C. This may be due to the fact that during the heating process, the particles tend to homogenize, resulting in a decrease of the average particle size, which is consistent with the change trend of the unit cell volume.

**Table 1.** Lattice parameters and particle average diameter of samples.

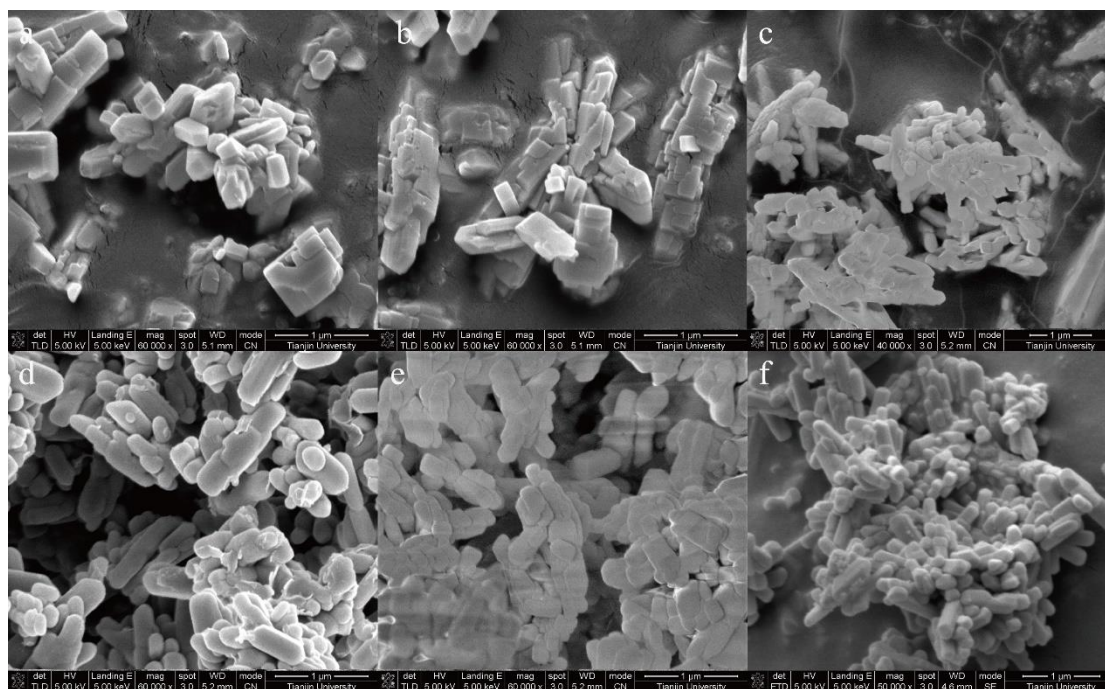
Sample	lattice parameters				The average particle size d/Å
	a/Å	b/Å	c/Å	V/Å <sup>3</sup>	
JCPDS no. 40-1499	6.0189	10.347	4.7039	292.95	
d	6.00535	10.3512	4.70493	292.47	621
e	6.00408	10.33479	4.71522	292.58	679
f	6.01003	10.35234	4.70566	292.78	831
g	6.01145	10.35586	4.70903	293.15	838
h	6.00881	10.35203	4.70545	292.69	720

Fig. 6 shows the FT-IR spectra of LiFePO<sub>4</sub> synthesized by hydrothermal stripping method. The absorption peak in the range of 982-1136 cm<sup>-1</sup> corresponds to the stretching vibration of the PO<sub>4</sub><sup>3-</sup> unit and the bands in the range of 440-550 cm<sup>-1</sup> are sensitive to the local lithium environment. FT-IR shows no absorption at 424 cm<sup>-1</sup>, indicating that there is no vibration signal of Li<sub>3</sub>PO<sub>4</sub> [25]. The spectrum indicates the intrinsic band of LiFePO<sub>4</sub>, without any poisoning of other impurity phases, which verifies the purity of the synthesized sample [26,27]. These findings confirm that hydrothermal stripping method can successfully synthesize pure LiFePO<sub>4</sub> nanoparticles.

Fig. 7 shows SEM images of samples synthesized at different temperatures and time. It can be observed that the particle morphology and size of the samples are strongly related to the temperature and time of the reaction. When the temperature was 160 °C or 180 °C, the morphology of samples (a) and (b) was blocky with uneven dimensions. As the temperature rose to 220 °C, the morphology of sample (c) gradually turns from block to rod, and the particle size tended to be evenly distributed. Fig. 7 (d-f) correspond to the SEM images of the products at 250 °C for different reaction time. When the reaction time was 1 h (d), it can be clearly seen that the edge of the particles were somewhat incomplete. When the reaction time was extended to 3 h, the edge of the particles tended to be intact and the crystals grow completely. The morphology and particle size of the obtained product (e) were basically consistent.



**Figure 6.** The infrared spectra of LiFePO<sub>4</sub>.



**Figure 7.** SEM of samples prepared at different reaction temperatures and time. (a) 160 °C, 3 h; (b) 180 °C, 3 h; (c) 220 °C, 3 h; (d) 250 °C, 1 h; (e) 250 °C, 3 h; (f) 250 °C, 5 h

Selected samples (a)-(c) with different morphologies and particle sizes shown in Table 2. Charge/discharge tests between 2.5 V and 4.2 V were carried out to study the influence of sample morphology and particle size on electrochemical performance. The initial charge-discharge voltage curves at 0.1 C are shown in Fig. 8A. The discharge platform of sample (a) which was blocky with uneven particle size was short and unstable. The discharge voltage of curve was low, indicating a high

degree of polarization. Samples (b) and (c) with uniform rod-shaped particles showed a very stable flat discharge voltage platform at about 3.4 V, which was caused by the intercalation/deintercalation of lithium ions and the related  $\text{Fe}^{3+}/\text{Fe}^{2+}$  conversion process [28]. The initial discharge capacities of samples (a)-(c) are 64.9, 148.0 and 151.6 mAh  $\text{g}^{-1}$ , respectively, indicating that the sample with regular morphology and small particle size have the highest discharge capacity in the first cycle.

Fig. 8B displays the rate capacities of the samples a-c at different current densities. It is obvious that sample (c) displays excellent rate cycling performance. Its discharge specific capacities at 0.1, 0.2, 0.5 and 1.0 C were the highest compared to other samples, which were 151.6, 153.9, 149.6 and 139.5 mAh  $\text{g}^{-1}$ . When it returned to 0.1 C after charging and discharging cycles at various current densities, the specific capacity of the sample reached 156.1 mAh  $\text{g}^{-1}$ , which was close to the theoretical capacity (170.0 mAh  $\text{g}^{-1}$ ). It has excellent rate discharge capacity compared with other  $\text{LiFePO}_4$ -based electrode materials reported in the literature [9, 29-32], as shown in Table 3. Compared with the initial 0.1 C cycle, the increase in capacity can be explained as the cycle of larger current increases the active surface area of the  $\text{LiFePO}_4$  cathode material, reduces the apparent current density, and reduces the polarization.

Cyclic Voltammetry (CV) test was performed to explore the reaction kinetics of the samples. Fig. 8C shows the corresponding curves of the samples (a)-(c) at 0.1 mV  $\text{s}^{-1}$ . All samples presented a pair of redox peaks at about 3.26 and 3.60 V, due to the  $\text{Li}^+$  intercalation/deintercalation process [33]. The oxidation peak is in the negative direction of the Y axis, and the reduction peak is in the positive direction. The sharper the peak, the greater the exchange current density of the material and the smaller the electrochemical impedance. The sample (c) displayed the highest redox currents, indicating the smallest electrochemical impedance.

EIS was performed on samples (a)-(c) to further compare the interfacial reaction resistance and the apparent  $\text{Li}^+$  ion diffusion coefficient (Fig. 8D). The semicircle in the high-to-middle frequency regime represents the charge transfer resistance ( $R_{ct}$ ).  $R_{ct}$  of sample (c) is 234  $\Omega$ , which is much lower than that of sample (a) (507  $\Omega$ ) and sample (b) (340  $\Omega$ ), indicating that the appropriate morphology and particle size can effectively improve the charge transfer ability of  $\text{LiFePO}_4$ . The sloping line at low frequency regime can be ascribed to  $\text{Li}^+$  diffusion [34,35]. Equivalent circuit model (inset of Fig. 8D) was used to fit the impedance spectra, where  $R_e$  represents the ohmic resistance,  $R_{ct}$  the charge-transfer resistance, CPE the constant phase elements and  $Z_W$  the Warburg impedance.  $\text{Li}^+$  diffusion coefficient ( $\text{D}/\text{cm}^2 \text{ s}^{-1}$ ) can be calculated by the following formula (4) [36],

$$D = \frac{R^2 T^2}{2A^2 F^4 n^4 c^2 \sigma^2} \quad (4)$$

where R is the gas constant, T is absolute temperature, A is electrode surface areas, n is the transferred electron number,  $\sigma$  is the slope of the fitted line  $Z' \sim \omega^{-1/2}$ , F is the Faraday's constant, C is  $\text{Li}^+$  concentration. According to the above formula, the D values of samples (a)-(c) are  $1.46 \times 10^{-14}$ ,  $8.50 \times 10^{-15}$ ,  $7.04 \times 10^{-14} \text{ cm}^2 \text{ s}^{-1}$ , respectively. Analysis shows that sample (c) has the highest lithium ion diffusion coefficient and the smallest charge transfer resistance. This result further confirms that the sample with regular morphology and small particle size can significantly promote the  $\text{Li}^+$  diffusion rate and charge transfer ability of  $\text{LiFePO}_4$  as a cathode material for lithium-ion batteries, demonstrating its excellent capacity and rate performance.

**Table 2.** Samples with different morphologies and particle sizes.

Sample	Morphology	The average particle size d/nm	Synthesis conditions
a	Blocky, uneven	62.1	160 °C, 3 h
b	Rod-shaped, uniform	83.8	220 °C, 3 h
c	Rod-shaped, uniform	72.0	250 °C, 3 h

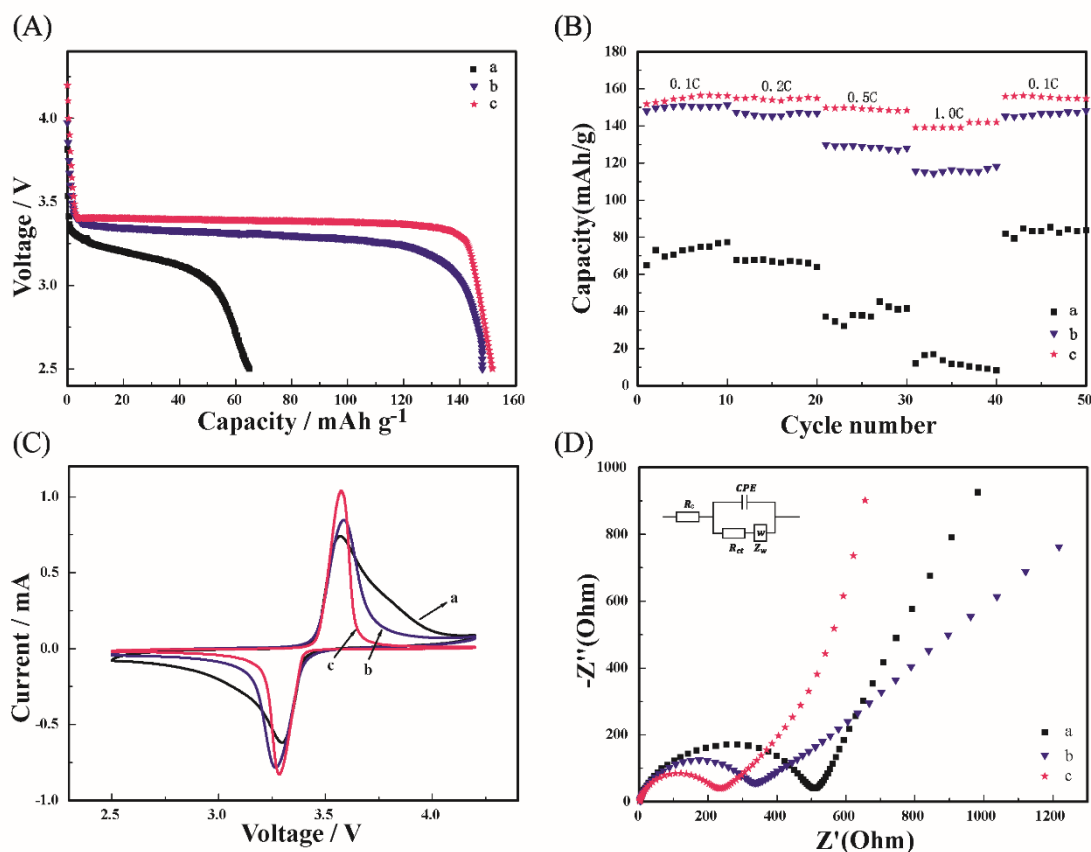


**Figure 8.** Initial charge-discharge curves at 0.1 C (A), specific charge and discharge capacities at various current rates (B), cyclic voltammograms (C) and electrochemical impedance spectroscopy (D) of LiFePO<sub>4</sub> samples with different morphologies and particle sizes.

**Table 3.** Comparison the material presented in this paper with other LiFePO<sub>4</sub>-based electrode materials for lithium-ion batteries reported previously.

Electrode materials	Particle morphology	Discharge capacities(mA h/g)				Reference
		0.1 C	0.2 C	0.5 C	1.0 C	
LiFePO <sub>4</sub>	Rod-shaped	151.6	153.9	149.6	139.5	This work
LiFePO <sub>4</sub> /C	Cluster texture	---	152.3	150	142.2	[9]
LiFePO <sub>4</sub> /C	nanoplate	123.0	117	106	90	[29]
LiFePO <sub>4</sub> -PANI	Blocky	145	---	130	117	[30]
LiFePO <sub>4</sub> /TiO <sub>2</sub>	nanocomposite	---	137.7	134.9	123.5	[31]
Cl-doped LiFePO <sub>4</sub> /C	nanoparticle	151	146	134	130	[32]

#### 4. CONCLUSIONS

In the present work, we have applied a simple, energy-efficient, cost-effective, green route for the synthesis of LiFePO<sub>4</sub> cathode materials. Inexpensive industrial-grade FeSO<sub>4</sub>·7H<sub>2</sub>O can be used as a raw material. In the aqueous phase, the Li<sup>+</sup>/PO<sub>4</sub><sup>3-</sup> molar ratio is controlled to 1.2:1, the pH is adjusted to be acidic or neutral, and an appropriate amount of reducing agent is added to synthesize pure LiFePO<sub>4</sub> nanoparticles. By changing the temperature and time of hydrothermal stripping method, LiFePO<sub>4</sub> samples with different morphologies and particle sizes can be prepared. By comparing the electrochemical properties of samples with different morphologies and particle sizes, it was found that LiFePO<sub>4</sub> nanoparticles with regular morphology and small size have the best electrochemical performance, offering a high discharge capacity of 156.1 mAh g<sup>-1</sup> at 0.1 C after 40 cycles. The hydrothermal stripping method not only has the advantages of hydrothermal synthesis process but also overcomes the issues of high cost and difficult control of the reaction. Therefore, the hydrothermal stripping method is expected to have a very good prospects for large-scale production.

#### ACKNOWLEDGMENTS

This work was supported by the National Natural Science Foundation of China (No. 21276185).

#### CONFLICT OF INTEREST

We declare no conflict of interest.

#### References

1. J. J. Wang and X. L. Sun, *Energ. Environ. Sci.*, 8 (2015) 1110.
2. P. P. Prosini, M. Carewska, S. Scaccia, P. Wisniewski and M. Pasquali, *Electrochim. Acta*, 48 (2003) 4205.
3. G. Jeong, Y. U. Kim, H. Kim, Y. J. Kim and H. J. Sohn, *Energ. Environ. Sci.*, 4 (2011) 1986.
4. J. F. Qian, M. Zhou, Y. L. Cao, X. P. Ai and H. X. Yang, *J. Phys. Chem. C*, 114 (2010) 3477.
5. F. Yu, J. J. Zhang, Y. F. Yang and G. Z. Song, *J. Power Sources*, 195 (2010) 6873.
6. X. M. Lou and Y. X. Zhang, *J. Mater. Chem.*, 21 (2011) 4156.
7. R. Dominko, M. Bele, M. Gaberscek, M. Remskar, D. Hanzel, J. M. Goupil, S. Pejovnik and J. Jamnik, *J. Power Sources*, 153 (2006) 274.
8. M. Rastgoo-Deylami, M. Javanbakht, M. Ghaemi, L. Naji, H. Omidvar and M. R. Ganjali, *Int. J. Electrochem. Sci.*, 9 (2014) 3199.
9. Y. C. Yao, X. P. Huang, D. Zhou, B. Yang, W. H. Ma and F. Liang, *Int. J. Electrochem. Sci.*, 14 (2019) 2442.
10. S. N. Zhao, L. Wen, J. L. Liu, J. Q. Chen and F. L. Bei, *Int. J. Electrochem. Sci.*, 15 (2020) 8873.
11. A. Yamada and S. C. Chung, *J. Electrochem. Soc.*, 148 (2001) A960.
12. B. Kang and G. Ceder, *Nature*, 458 (2009) 190.
13. D. Li, Y. D. Huang, N. Sharma, Z. X. Chen, D. Z. Jia and Z. P. Guo, *Phys. Chem. Chem. Phys.*, 14 (2012) 3634.
14. X. H. Yang, J. G. Tu, M. Lei, Z. C. Zuo, B. R. Wu and H. H. Zhou, *Electrochim Acta*, 193 (2016) 206.
15. A. V. Murugan, T. Muraliganth and A. Manthiram, *J. Electrochem. Soc.*, 156 (2009) A79.

16. B. Q. Zhu, X. H. Li, Z. X. Wang and H. J. Guo, *Mater. Chem. Phys.*, 98 (2006) 373.
17. M. Justel, A. Schwinger, B. Friedrich and M. Binnewies, *Z. Phys. Chem.*, 226 (2012) 177.
18. J. Lee and A. S. Teja, *J. Supercrit. Fluid.*, 35 (2005) 83.
19. S. F. Yang, P. Y. Zavalij and M. S. Whittingham, *Electrochem. Commun.*, 3 (2001) 505.
20. J. L. Liu, R. R. Jiang, X. Y. Wang, T. Huang and A. S. Yu, *J. Power Sources*, 194 (2009) 536.
21. A. Kuwahara, S. Suzuki and M. Miyayama, *J. Electroceram.*, 24 (2010) 69.
22. B. Ellis, W. H. Kan, W. R. M. Makahnouk and L. F. Nazar, *J. Mater. Chem.*, 17 (2007) 3248.
23. N. Ravet, M. Gauthier, K. Zaghbi, J. B. Goodenough, A. Mauger, F. Gendron and C. M. Julien, *Chem. Mater.*, 19 (2007) 2595.
24. J. F. Ni, M. Morishita, Y. Kawabe, M. Watada, N. Takeichi and T. Sakai, *J. Power Sources*, 195 (2010) 2877.
25. S. P. Wang, C. G. Zhou, Q. A. Zhou, G. Ni and J. P. Wu, *J. Power Sources*, 196 (2011) 5143.
26. K. Shiraishi, K. Dokko and K. Kanamura, *J. Power Sources*, 146 (2005) 555.
27. Z. Y. Sui, X. T. Zhang, Y. Lei and Y. J. Luo, *Carbon*, 49 (2011) 4314.
28. Y. K. Zhou, J. Wang, Y. Y. Hu, R. O'Hayre and Z. P. Shao, *Chem. Commun.*, 46 (2010) 7151.
29. S. J. Sun, Q. L. An, Z. Q. Tian, X. Y. Zhao and X. D. Shen, *Energy Fuels*, 34 (2020) 11597.
30. C. Ajpi, N. Leiva, M. Vargas, A. Lundblad, G. Lindbergh and S. Cabrera, *Materials (Basel)*, 13 (2020) 2834.
31. P. Q. Hou, S. N. Li, L. Yang, Y. F. Wang, L. X. Wang and S. H. Luo, *Ionics*, 26 (2020) 2139.
32. H. Liu, S. H. Luo, S. X. Yan, Y. F. Wang, Q. Wang, M. Q. Li and Y. H. Zhang, *J. Electroanal. Chem.*, 850 (2019) 113434.
33. J. M. Lu, Y. K. Zhou, T. T. Jiang, X. H. Tian, X. F. Tu and P. C. Wang, *Ceram. Int.*, 42 (2016) 1281.
34. B. Wang, T. F. Liu, A. M. Liu, G. J. Liu, L. Wang, T. T. Gao, D. L. Wang and X. S. Zhao, *Adv. Energy Mater.*, 6 (2016) 1600426.
35. Y. Zhang, W. C. Wang, P. H. Li, Y. B. Fu and X. H. Ma, *J. Power Sources*, 210 (2012) 47.
36. L. Yao, Y. Wang, J. H. Wu, M. W. Xiang, J. L. Li, B. Y. Wang, Y. Zhang, H. Wu and H. Liu, *Int. J. Electrochem. Sci.*, 12 (2017) 206.

© 2021 The Authors. Published by ESG ([www.electrochemsci.org](http://www.electrochemsci.org)). This article is an open access article distributed under the terms and conditions of the Creative Commons Attribution license (<http://creativecommons.org/licenses/by/4.0/>).